Journal of Organometallic Chemistry, 408 (1991) 7–18
Elsevier Sequoia S.A., Lausanne
JOM 21533

Synthesis and molecular structure of the borido cluster $Fe_4(CO)_{12}BHAu_2\{AsPh_3\}_2$ and an investigation of the electrochemistry of $Fe_4(CO)_{12}BHAu_2L_2$, L = $AsPh_3$ or PPh_3

Catherine E. Housecroft, Musa S. Shongwe
University Chemical Laboratory, Lensfield Road, Cambridge CB2 1EW (UK)

Arnold L. Rheingold
Department of Chemistry, University of Delaware, Newark, DE 19716 (USA)

and Piero Zanello
Dipartimento di Chimica, Università di Siena, 53100 Siena (Italy)

(Received October 15th, 1990)

Abstract

The synthesis and characterisation by X-ray crystallography of $Fe_4(CO)_{12}BHAu_2\{AsPh_3\}_2$ are reported. $Fe_4(CO)_{12}BHAu_2\{AsPh_3\}_2$ is isostructural with its phosphine analogue $Fe_4(CO)_{12}BHAu_2\{PPh_3\}_2$ and possesses a central Fe_4-butterfly framework with a semi-interstitial boron atom and two asymmetrically positioned $AuAsPh_3$ groups, one bridging an Fe_{wing}–B edge and one interacting with an Fe_{hinge}–B edge. Changing the gold(I) substituent from PPh_3 to $AsPh_3$ is sufficient to cause a significant difference in the redox behaviour of the auraferraborane clusters. Each of $Fe_4(CO)_{12}BHAu_2\{AsPh_3\}_2$ and $Fe_4(CO)_{12}BHAu_2\{PPh_3\}_2$ is subject to a one-electron reduction and a one-electron oxidation, and the phosphine derivative can be oxidised further to the dication. The redox congeners are short lived, but the degradation products can regenerate the starting clusters by reversing the redox pattern.

Introduction

Recently, three of us [1] explored the structural consequences of varying the phosphine ligands, L and L′, in compounds of the type $Fe_4(CO)_{12}BHAu_2LL'$ (L = L′ or L ≠ L′). Two isomeric forms, **A** and **B**, have been characterized (Fig. 1) [1,2]; these are in equilibrium in solution and the percentage of each isomer is determined by the steric requirements of L and L′ [1]. Isomer **A** is favoured for bulky ligands and for $Fe_4(CO)_{12}BHAu_2LL'$ in which L and L′ exhibit a combined Tolman cone angle $\geq 290°$, only **A** is observed [1,3,4]. We have argued that, while electronic factors appear to control the aggregation of the gold(I) phosphine fragments around the boron atom, it is steric factors which dictate the exact geometry of the $\{Fe_4BAu_2\}$-cluster core [3]. The structural parameters for

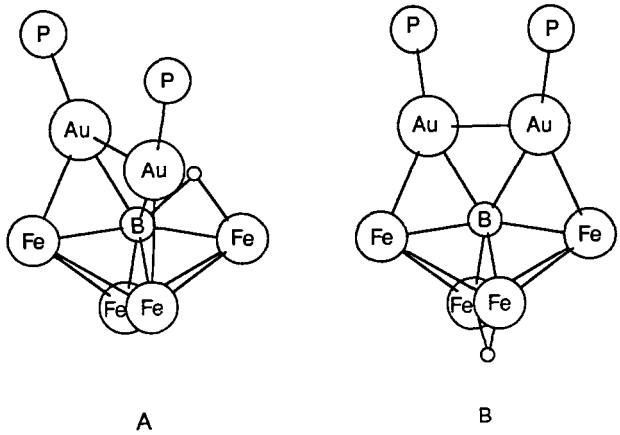

A B

Fig. 1. Schematic representations of isomers **A** and **B** of $Fe_4(CO)_{12}BHAu_2LL'$ (L and L' = phosphine); carbonyl ligands are omitted for clarity and the phosphine ligand is represented by the P atom only.

$Fe_4(CO)_{12}BHAu_2\{PPh_3\}_2$ (**1**) and $Fe_4(CO)_{12}BHAu_2\{P(p\text{-}MeC_6H_4)_3\}_2$ are very similar [1,3,4]; the Tolman cone angles [5] for PPh_3 and $P(p\text{-}MeC_6H_4)_3$ are identical (145°) although the σ-donor ability of $P(p\text{-}MeC_6H_4)_3$ is slightly greater than that of PPh_3 [6]. In order to extend this series, we have prepared and structurally characterized $Fe_4(CO)_{12}BHAu_2\{AsPh_3\}_2$ (**2**) and have investigated the electrochemistry of both this and its phosphino analogue **1**.

Experimental

General data

The preparations of **1** and **2** were carried out under an inert atmosphere by standard Schlenk techniques. Solvents were dried and redistilled before use. $Ph_3AsAuCl$ was prepared by a literature method [7]; compound **1** [3,4] and $[PPN][HFe_4(CO)_{12}BH]$ [8], (PPN = bis(triphenylphosphine)nitrogen(1+)), were prepared as previously reported. FT-NMR spectra were recorded on a Bruker AM 400 spectrometer. ^1H NMR chemical shifts are with respect to $\delta = 0$ for Me_4Si, ^{11}B NMR with respect to $\delta = 0$ for $F_3B \cdot OEt_2$. All downfield chemical shifts are positive. Infrared spectra were recorded on a Perkin–Elmer FT 1710 spectrophotometer. FAB mass spectra were recorded on a Kratos MS 890 instrument.

$Fe_4(CO)_{12}BHAu_2\{AsPh_3\}_2$ (2)

Solid $[PPN][HFe_4(CO)_{12}BH]$ (0.15 g, 0.14 mmol) was combined with $Ph_3AsAuCl$ (0.15 g, 0.28 mmol) and excess $TlPF_6$ (0.14 g, 0.41 mmol). To this was added CH_2Cl_2 (20 ml) in which all reagents dissolved. The solution was stirred for 45 min after which Et_2O (8 ml) was added to precipitate $[PPN][PF_6]$, TlCl and excess $TlPF_6$. After filtration, solvent was removed in vacuo from the filtrate. The residue was redissolved in CH_2Cl_2 and the product separated by centrifugal chromatography as the second, dark green band (90% yield). **2**: 250 MHz ^1H NMR (CD_2Cl_2) δ 7.7–7.5 (m, Ph), −9.9 (br, Fe-*H*-B); 128 MHz ^{11}B NMR (CD_2Cl_2) δ +138.0 (J(BH) ≈ 80 Hz from line-width analysis); IR (CH_2Cl_2, cm^{-1}) ν(CO) 2058m, 2020vs, 1996vs,

1970sh; FAB-MS (NOBA matrix) m/z 1578 (P^+) with stepwise loss of 12 CO; elem. anal. Found (calc.) (%): C, 36.20 (36.50); H, 1.99 (1.96).

Crystal structure determination

A dark brown crystal suitable for X-ray analysis was grown from CH_2Cl_2 layered with hexane and light petroleum ether. The crystal and data collection parameters are summarised in Table 1. The centrosymmetric space group $P\bar{1}$ was assumed correct throughout; the chemically reasonable results indicate this was the correct choice. An empirical, ψ-scan correction for absorption was applied to the data.

A Patterson map was used to locate the Au-atom positions. During refinement, the phenyl rings were constrained to rigid, planar hexagons. All non-hydrogen atoms were refined with anisotropic thermal parameters and the hydrogen atoms were treated as idealised, isotropic contributions.

SHELXTL (5.1) software was used for all the calculations (Nicolet XRD, Madison, WI). Atomic coordinates are given in Table 2 and selected bond distances and angles in Table 3. Structure factor tables (37 pages) may be obtained from the authors (A.L.R.)

Electrochemistry

The electrochemical apparatus has been described elsewhere [9]. Anhydrous CH_2Cl_2 (Aldrich gold label) was used as received. Tetra-n-butylammonium hexa-

Table 1

Crystallographic data for **2**

Crystal parameters:			
Formula	$C_{48}H_{31}As_2Au_2BFe_4O_{12}$	γ, °	73.42(1)
Formula weight	1577.47	V, Å^3	2610.3(9)
Crystal system	triclinic	Z	2
Space group	$P\bar{1}$	Cryst. dimens., mm	0.28×0.30×0.32
a, Å	10.948(2)	Cryst. colour	dark brown
b, Å	12.239(2)	D(calc), g cm^{-3}	2.007
c, Å	20.718(5)	μ(Mo-K_α), cm^{-1}	79.85
α, °	79.68(2)	Temp., K	296
β, °	83.00(2)	T(max)/T(min)	2.36
Data collection:			
Diffractometer	Nicolet R3m	Indpt. reflections	9196
Monochromator	graphite	R(merg), %	2.20
Radiation	Mo-K_α	Indpt. obs. reflections $F_o \geq n\sigma(F_o)$	6240 ($n = 5$)
2θ-scan range, °	4–50	Std. reflections	3 std/197 reflections
Data collected (h,k,l)	±14,±15,25	Var. in stds.	< 3.5
Reflections collected	9473		
Refinement:			
$R(F)$, %	4.54	$\Delta(\rho)$, e Å^{-3}	1.58
$R(wF)$, %	5.48	N_o/N_v	11.3
Δ/σ(max)	0.09	*GOF*	1.165

Table 2

Atomic coordinates ($\times 10^4$) and isotropic thermal parameters ($Å^2 \times 10^3$) for **2**

Atom	x	y	z	U^a
Au(1)	906.4(4)	3315.4(4)	1943.2(2)	55.6(2)
Au(2)	2839.3(4)	2574.5(3)	2909.0(2)	50.4(2)
As(1)	1616(1)	2333.2(9)	1001.0(5)	52.2(4)
As(2)	4496(1)	787.0(9)	3046.8(5)	50.9(4)
Fe(1)	−884(1)	4670(1)	2613.7(8)	52.0(6)
Fe(2)	−189(2)	4580(1)	3775.7(8)	57.0(6)
Fe(3)	−726(1)	2737(1)	3486.7(8)	54.3(6)
Fe(4)	1557(1)	4725(1)	2735.3(7)	49.4(5)
B	656(12)	3500(11)	3060(6)	56(5)
O(1)	−2739(10)	6434(8)	3262(5)	111(5)
O(2)	−876(11)	6361(8)	1430(5)	111(5)
O(3)	−2736(10)	3841(10)	2030(6)	67(5)
O(4)	1798(8)	3160(8)	4636(4)	88(4)
O(5)	−2275(10)	4557(10)	4826(5)	116(6)
O(6)	−86(10)	6853(8)	4029(5)	108(5)
O(7)	−3508(8)	3611(9)	3729(6)	112(5)
O(8)	−296(9)	1385(8)	4791(5)	96(5)
O(9)	−826(10)	898(8)	2788(5)	99(5)
O(10)	3418(10)	4772(8)	3613(5)	100(5)
O(11)	3306(10)	4910(8)	1570(5)	104(5)
O(12)	487(9)	7248(7)	2503(5)	97(5)
C(1)	−1948(12)	5668(10)	3090(7)	77(5)
C(2)	−839(11)	5680(10)	1917(6)	69(5)
C(3)	−2048(13)	4123(10)	2253(7)	87(6)
C(4)	1033(11)	3715(11)	4304(5)	70(5)
C(5)	−1488(12)	4540(10)	4402(6)	71(5)
C(6)	−116(12)	5969(11)	3924(6)	72(5)
C(7)	−2426(12)	3292(11)	3622(7)	81(6)
C(8)	−486(12)	1921(10)	4288(7)	69(5)
C(9)	−804(11)	1629(10)	3049(6)	67(5)
C(10)	2726(11)	4726(9)	3259(6)	64(5)
C(11)	2615(11)	4788(9)	2003(6)	67(5)
C(12)	831(11)	6253(10)	2592(6)	70(5)
C(21)	4002(7)	2919(7)	683(3)	69(5)
C(22)	4919	3376	288	87(7)
C(23)	4729	3820	−471	92(7)
C(24)	3623	3808	−636	78(6)
C(25)	2706	3351	−242	68(5)
C(26)	2895	2906	418	55(4)
C(31)	331(7)	1606(5)	57(4)	67(5)
C(32)	−611	1769	−375	83(6)
C(33)	−1580	2800	−445	75(6)
C(34)	−1606	3667	−85	83(6)
C(35)	−663	3503	347	71(5)
C(36)	305	2472	417	57(4)
C(41)	2018(8)	26(7)	1720(4)	76(6)
C(42)	2569	−1163	1836	96(7)
C(43)	3519	−1689	1391	86(7)
C(44)	3919	−1027	828	97(7)
C(45)	3369	162	712	83(6)
C(46)	2418	688	1157	61(5)
C(51)	6331(8)	1380(6)	2053(4)	78(6)

Table 2 (*continued*)

Atom	*x*	*y*	*z*	U^a
C(52)	7199	1264	1501	99(8)
C(53)	7420	308	1181	115(9)
C(54)	6772	−533	1412	138(11)
C(55)	5904	−416	1964	103(8)
C(56)	5684	540	2284	57(4)
C(61)	2487(6)	−343(5)	3403(4)	60(5)
C(62)	1963	−1266	3635	81(6)
C(63)	2761	−2382	3765	80(6)
C(64)	4084	−2575	3663	87(6)
C(65)	4608	−1652	3431	79(6)
C(66)	3810	−536	3302	58(4)
C(71)	5134(7)	1322(7)	4239(4)	82(6)
C(72)	5865	1183	4769	110(9)
C(73)	7060	379	4796	117(10)
C(74)	7524	−285	4293	111(9)
C(75)	6794	−145	3762	77(6)
C(76)	5598	658	3735	60(5)

[a] Equivalent isotropic U defined as one third of the trace of the orthogonalized U_{ij} tensor.

fluorophosphate supporting electrolyte (Aldrich) was stored in a vacuum oven. All potential values refer to the saturated calomel electrode. Against this electrode, the ferrocene/ferrocinium couple is observed at +0.49 V.

Results and discussion

Structure of $Fe_4(CO)_{12}BHAu_2\{AsPh_3\}_2$ (2)

The full molecular structure of **2** is shown in Fig. 2 and, for clarity, the core atoms only are depicted in Fig. 3. Selected bond lengths and angles are listed in Table 3. The four iron atoms in **2** define a butterfly, the parameters of which are similar to those in **1**; the internal dihedral angle of **2** is 113.6(3)° compared to 113.4(3)° in **1** [3] and the boron atom resides 0.32(2) Å above the Fe_{wing}—Fe_{wing} axis and this compares with 0.37(1) Å in **1** [3]. Thus, compound **2** provides the fourth example in a series of auraferraboranes which, upon exchange of two protons for two gold(I) electrophiles, not only simply retain the Fe_4B-core of the parent cluster $HFe_4(CO)_{12}BH_2$ [10,11], but do so with minimal structural perturbation of this five atom unit. The two $\{AuAsPh_3\}$-fragments in **2** are sited asymmetrically with respect to the Fe_4B-core; Au(2) bridges a wingtip iron–boron atom edge (viz. Fe(4)–B) while Au(1) bridges a hinge iron–boron atom edge (viz. Fe(1)–B). The distance Au(1)–Fe(4) is significantly longer (2.860(2) Å) than the other iron–gold atom separations (2.613(1) and 2.590(1) Å) and thus we consider Au(1) to be edge bridging rather than face capping (see Fig. 3). This arrangement of gold(I) moieties replicates that in **1**; we have previously noted in **1** that the generation of an Fe_{hinge}–Au(L)–B interaction necessarily causes the associated hinge iron tricarbonyl unit to undergo a 60° rotation with respect to its orientation in the parent compound $HFe_4(CO)_{12}BH_2$ [1,3,4]. This feature is again observed in **2** and C(1)O(1) becomes semi-bridging across the hinge bond, Fe(1)–Fe(2). Thus, in the solid state,

Table 3

Selected bond lengths (Å) and angles (°) for **2**

Au(1)–Au(2)	2.931(1)	Au(1)–As(1)	2.408(1)
Au(1)–Fe(1)	2.613(1)	Au(1)–Fe(4)	2.860(2)
Au(1)–B	2.341(13)	Au(2)–As(2)	2.408(1)
Au(2)–Fe(4)	2.590(1)	Au(2)–B	2.344(12)
Fe(1)–Fe(2)	2.586(2)	Fe(1)–Fe(3)	2.685(2)
Fe(1)–Fe(4)	2.734(2)	Fe(1)–B	2.068(11)
Fe(2)–Fe(3)	2.668(3)	Fe(2)–Fe(4)	2.717(2)
Fe(2)–B	2.114(13)	Fe(3)–B	2.031(14)
Fe(4)–B	1.999(14)		
Au(2)–Au(1)–As(1)	111.0(1)	Au(2)–Au(1)–Fe(1)	98.4(1)
As(1)–Au(1)–Fe(1)	150.4(1)	Au(2)–Au(1)–Fe(4)	53.1(1)
As(1)–Au(1)–Fe(4)	143.8(1)	Fe(1)–Au(1)–Fe(4)	59.7(1)
Au(2)–Au(1)–B	51.3(3)	As(1)–Au(1)–B	156.1(3)
Fe(1)–Au(1)–b	49.0(3)	Fe(4)–Au(1)–B	43.8(4)
Au(1)–Au(2)–As(2)	127.4(1)	Au(1)–Au(2)–Fe(4)	62.0(1)
As(2)–Au(2)–Fe(4)	165.0(1)	Au(1)–Au(2)–B	51.2(3)
As(2)–Au(2)–B	146.9(3)	Fe(4)–Au(2)–B	47.5(3)
Au(1)–Fe(1)–Fe(2)	110.2(1)	Au(1)–Fe(1)–Fe(3)	83.5(1)
Fe(2)–Fe(1)–Fe(3)	60.8(1)	Au(1)–Fe(1)–Fe(4)	64.6(1)
Fe(2)–Fe(1)–Fe(4)	61.3(1)	Fe(3)–Fe(1)–Fe(4)	94.2(1)
Au(1)–Fe(1)–B	58.6(4)	Fe(2)–Fe(1)–B	52.6(4)
Fe(3)–Fe(1)–B	48.5(4)	Fe(4)–Fe(1)–B	46.7(4)
Fe(1)–Fe(2)–Fe(3)	51.4(1)	Fe(1)–Fe(2)–Fe(4)	62.0(1)
Fe(3)–Fe(2)–Fe(4)	95.0(1)	Fe(1)–Fe(2)–B	51.0(3)
Fe(3)–Fe(2)–B	48.6(4)	Fe(4)–Fe(2)–B	46.9(4)
Fe(1)–Fe(3)–Fe(2)	57.8(1)	Fe(1)–Fe(3)–B	49.7(3)
Fe(2)–Fe(3)–B	51.3(4)	Au(1)–Fe(4)–Au(2)	64.9(1)
Au(1)–Fe(4)–Fe(1)	55.6(1)	Au(2)–Fe(4)–Fe(1)	104.1(1)
Au(1)–Fe(4)–Fe(2)	99.7(1)	Au(2)–Fe(4)–Fe(2)	96.7(1)
Fe(1)–Fe(4)–Fe(2)	56.6(1)	Au(1)–Fe(4)–B	54.2(4)
Au(2)–Fe(4)–B	59.8(3)	Fe(1)–Fe(4)–B	48.8(3)
Fe(2)–Fe(4)–b	50.5(4)	Au(1)–B–Fe(1)	72.4(4)
Au(2)–B–Fe(1)	144.3(6)	Au(1)–B–Au(2)	77.4(4)
Au(1)–B–Fe(2)	146.3(6)	Au(2)–B–Fe(2)	125.5(7)
Fe(1)–B–Fe(2)	76.4(4)	Au(1)–B–Fe(3)	107.3(7)
Au(2)–B–Fe(3)	126.0(6)	Fe(1)–B–Fe(3)	81.8(5)
Fe(2)–B–Fe(3)	80.1(4)	Au(1)–B–Fe(4)	82.0(4)
Au(2)–B–Fe(4)	72.7(4)	Fe(1)–B–Fe(4)	84.5(5)
Fe(2)–B–Fe(4)	82.6(5)	Fe(3)–B–Fe(4)	160.1(7)

the triphenylarsine and triphenylphosphine derivatives of $HFe_4(CO)_{12}BHAu_2L_2$ are isostructural.

Solution structure of **2**. The *endo*-hydrogen atom in **2** was not located but is proposed on the basis of solution spectroscopic data to lie along the edge Fe(3)–B. The ^1H NMR chemical shift of δ −9.9 and the observed ^1H–^{11}B coupling ($J_{BH} \approx 80$ Hz) imply the presence of an Fe–H–B bridging interaction. The highfield ^1H NMR resonance is temperature invariant on the 250 MHz time scale, and this implies that **2** exhibits one solution structure, namely **A** in Fig. 1. Based on data from a series of phosphino derivatives [1], the ^{11}B NMR shift of +138.0 is also consistent with a single isomer for **2**. Since the Tolman cone angle for $AsPh_3$ is 147°

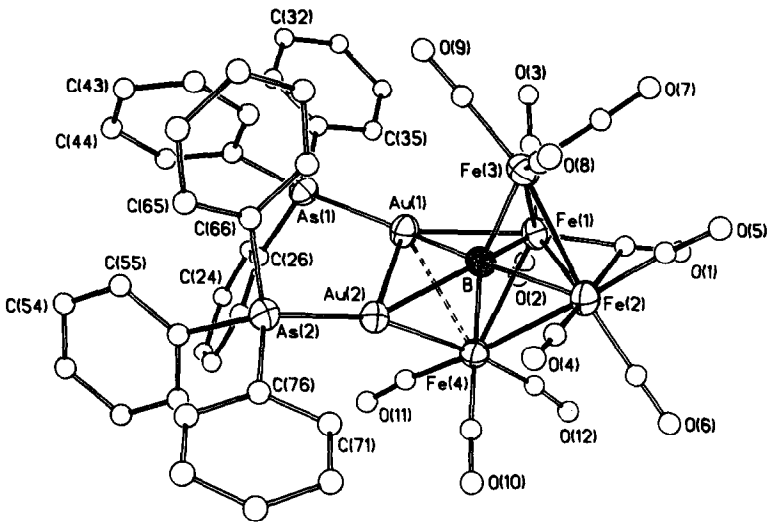

Fig. 2. Molecular structure of $Fe_4(CO)_{12}BHAu_2\{AsPh_3\}_2$ (**2**). The carbon atoms are drawn as arbitrary-size spheres to enhance clarity.

[5] i.e. similar to that for PPh_3, the observation of a single solution species for **2** is consistent with results for the phosphino derivatives [1].

Electrochemistry of 2

A transition metal cluster compound exhibits at its core an aggregate of atoms which is potentially redox active. However, compared to the enormous number of molecular clusters now characterised, studies of their electrochemistry are still few [12,13]. A preliminary electrochemical investigation of compound **2** prompted us to study the compound in detail and to compare the electrochemistry of this arsine derivative with that of its phosphine analogue, **1**. The ability of **2** to lose or gain electrons was initially investigated by cyclic voltammetry. Figure 4 shows the cathodic portion of the cyclic voltammetric response exhibited by **2** in dichloro-

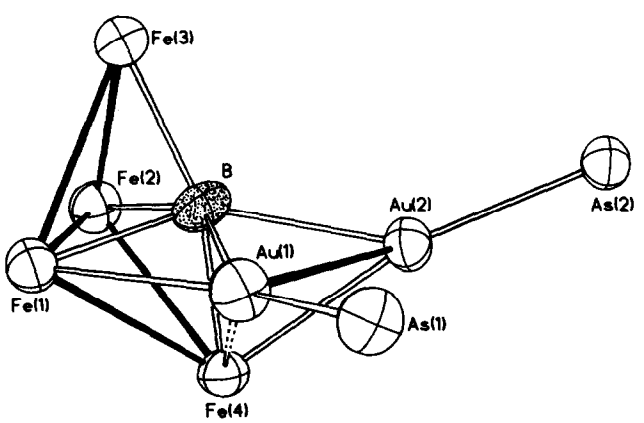

Fig. 3. The $\{Fe_4BAu_2As_2\}$-core structure of **2** emphasising the Fe_4-butterfly framework.

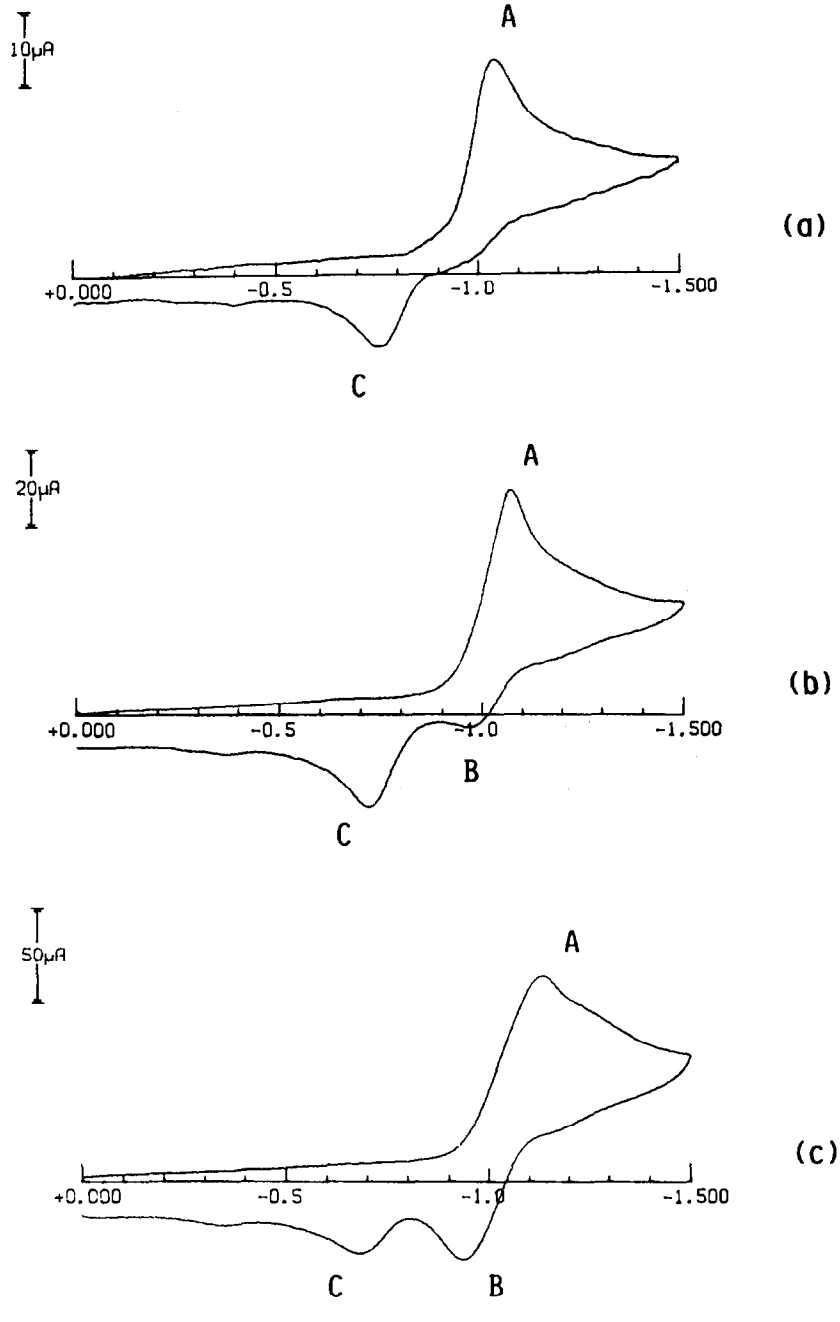

Fig. 4. Cathodic portion of the cyclic voltammetric response recorded at a platinum electrode in a deaerated CH_2Cl_2 solution containing **2** (1.0×10^{-3} mol dm^{-3}) and $[Bu_4N][PF_6]$ (0.1 mol dm^{-3}); (a) 0.2 V s^{-1}; (b) 1.00 V s^{-1}; (c) 5.12 V s^{-1}.

methane solution at different scan rates. The auraferraborane cluster undergoes a cathodic reduction corresponding to peak A. The characteristics of the return wave vary as a function of the scan rate. At low scan rate (Fig. 4a), the reduction step is accompanied by a reoxidation (peak C) which is not directly associated with peak A. At higher scan rates (Figs. 4b and 4c), a new peak, B, which is related to peak A, appears and the relative intensity of peak C decreases accordingly. Controlled potential coulometric tests (working potential = −1.3 V) indicate that the cathodic process involves a one-electron reduction. Analysis [13] of the cyclic voltammetric responses with scan rate v varying from 0.02 to 20.48 V s^{-1} shows that (i) the ratio $i_{p(B)}/i_{p(A)}$ progressively increases from 0.3 at 1.00 V s^{-1} to 1.0 at 10.24 V s^{-1}, (ii) the difference $E_{p(B)} - E_{p(A)} = \Delta E_p$ increases from 104 mV at 1.00 V s^{-1} to 272 mV at 20.48 V s^{-1}, and (iii) the term $i_{p(A)} \cdot v^{-1/2}$ remains practically constant. These parameters together are diagnostic of a one-electron redox change, quasi-reversible in character, and complicated by successive chemical changes. A formal electrode potential of −1.04 V can be assigned to the redox couple **2**/[**2**]$^-$. Peak C in Fig. 1 is assigned to the reoxidation of a byproduct which arises from decomposition of the primary electrogenerated monoanion [**2**]$^-$, the half life of which is approximately 0.1 s [14]. It is however worth noting that the species responsible for peak C is transient. In fact, a cyclic voltammogram run after exhaustive one-electron reduction only shows an irreversible oxidation peak at +0.2 V. Significantly, subsequent controlled potential electrolysis at +0.3 V regenerates the starting cluster **2**, so indicating that the cluster reorganisation/structural change that is induced by a one-electron addition is reversed upon one-electron oxidation.

The cyclic voltammogram in Fig. 5 shows the oxidation behaviour of **2**. Cyclic voltammetry coupled with controlled potential coulometry indicates that **2** undergoes a quasi-reversible one-electron oxidation which is complicated by subsequent chemical reaction. The monocation [**2**]$^+$ is relatively longer lived ($t_{1/2} \approx 3$ s) than [**2**]$^-$. A formal electrode potential of +0.69 V is determined for the couple [**2**]$^+$/**2**.

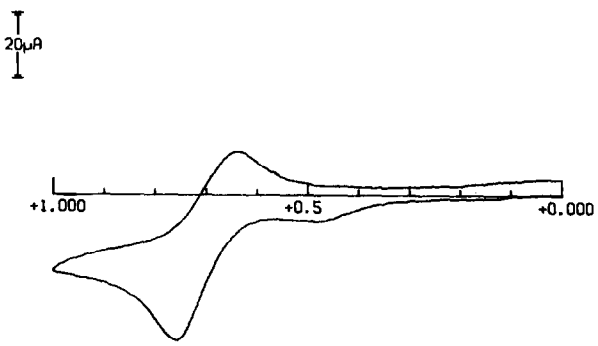

Fig. 5. Anodic portion of the cyclic voltammogram exhibited by **2** under the experimental conditions described in Fig. 4 with scan rate of 1.00 V s^{-1}.

Electrochemistry of 1

The rather interesting redox behaviour of **2** prompted us to investigate the electrochemistry of **1**. Figure 6 illustrates the cyclic voltammograms for **1** recorded in CH_2Cl_2 solution at the same scan rates as recorded in Fig. 4 for **2**. Like **2**, cluster **1** undergoes a one electron reduction which is complicated by chemical reaction.

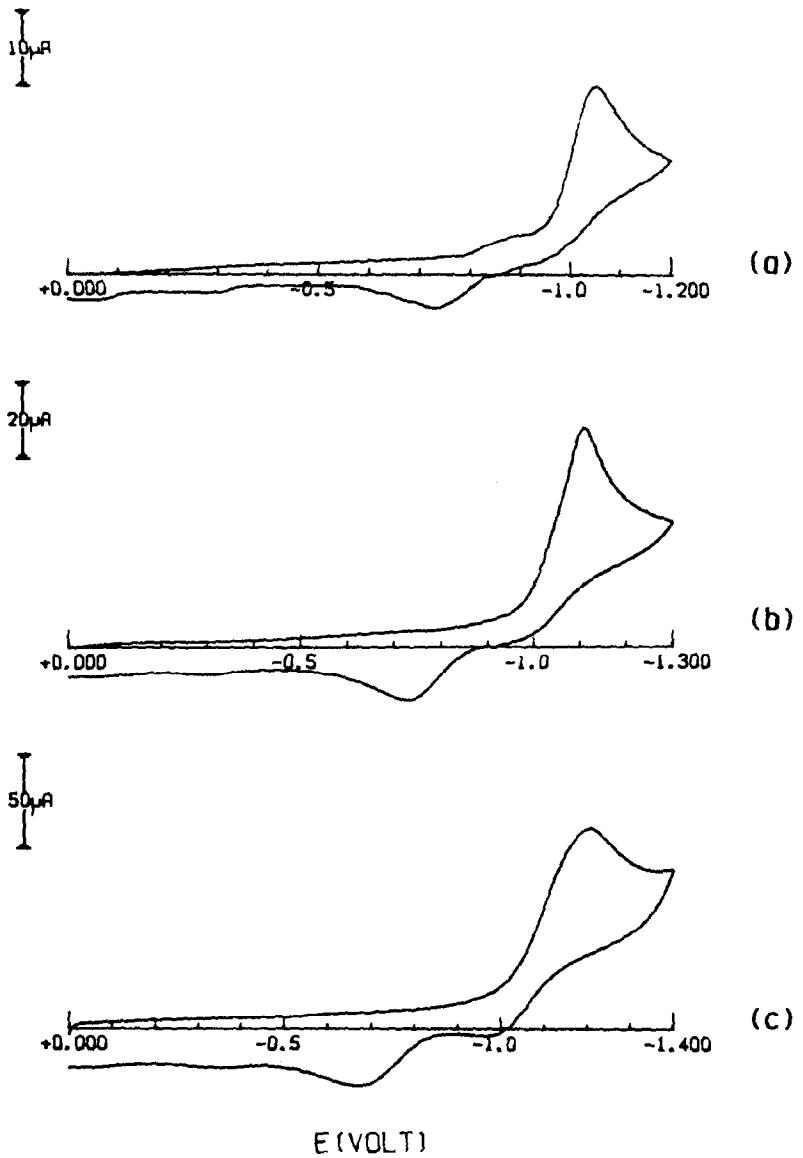

Fig. 6. Cathodic portion of the cyclic voltammograms recorded at a platinum electrode in a deaerated CH_2Cl_2 solution containing **1** (0.92×10^{-3} mol dm^{-3}) and $[Bu_4N][PF_6]$ (0.1 mol dm^{-3}); (a) 0.2 V s^{-1}; (b) 1.00 V s^{-1}; (c) 5.12 V s^{-1}.

Table 4

Comparison between the redox characteristics of $Fe_4(CO)_{12}BHAu_2\{AsPh_3\}_2$ (2) and $Fe_4(CO)_{12}BHAu_2\{AsPh_3\}_2$ (1) in CH_2Cl_2 solution

Compound	$E^{\circ}_{0/-}$ (V)	ΔE_p [a] (mV)	$t_{1/2(\text{monoanion})}$ [b] (s)
1	−1.10	284	0.01
2	−1.04	232	0.1
	$E^{0}_{+/0}$ (V)	ΔE_p [a] (mV)	$t_{1/2(\text{monocation})}$ [b] (s)
1	+0.39	297	0.05
2	+0.69	243	3
	$E^{\circ}_{2+/+}$ (V)	ΔE_p [a] (mV)	$t_{1/2(\text{dication})}$ [b] (s)
1	+0.65	283	1
2	–	–	–

[a] Measured at 10.24 V s^{-1}. [b] Approximate values.

However, in the case of **1**, these reactions are much faster and the half life of $[1]^-$ is significantly shorter than that of $[2]^-$ (Table 4). Nevertheless, the most significant difference between **1** and **2** lies in their anodic behaviour. As Fig. 7 shows, **1** undergoes two subsequent quasi-reversible one-electron oxidation steps, each one being coupled to a chemical reaction. The redox characteristics are listed in Table 4.

In conclusion, the electrochemistry of the borido clusters **1** and **2** illustrates that the metallic framework of the parent neutral compounds is flexible enough to permit both one-electron oxidation and reduction. Unfortunately, the lability of each of the monoanions and monocations mitigates against their isolation and structural characterization, but we have demonstrated that the chemical change that each undergoes affords a species which can revert to the starting cluster upon reversing the redox pathway. Differences in redox behaviour must stem from the identity of the gold ligands and, presumably, the electron donating ability thereof.

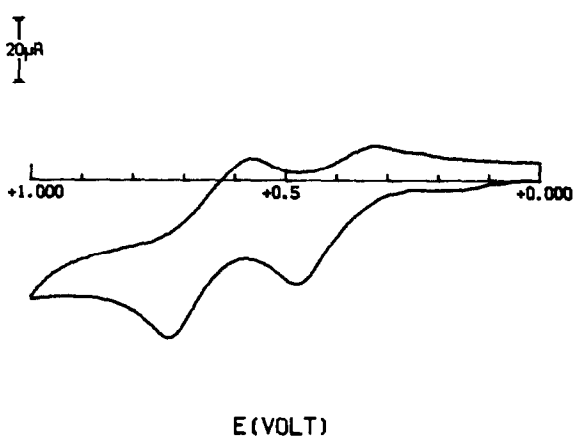

Fig. 7. Anodic portion of the cyclic voltammogram exhibited by **1** under the experimental conditions described in Fig. 6 with scan rate of 1.00 V s^{-1}.

Acknowledgements

We thank the Royal Society for a 1983 University Research Fellowship (to C.E.H.) and the Cambridge Commonwealth Trust and Tate and Lyle Corp. (to M.S.S.) N.S.F. is acknowledged for a grant towards the purchase of a diffractometer at the University of Delaware.

References

1 C.E. Housecroft, A.L. Rheingold and M.S. Shongwe, Organometallics, 8 (1989) 2651.
2 C.E. Housecroft, A.L. Rheingold and M.S. Shongwe, Organometallics, 7 (1988) 1885.
3 C.E. Housecroft and A.L. Rheingold, Organometallics, 6 (1987) 1332.
4 C.E. Housecroft and A.L. Rheingold, J. Am. Chem. Soc., 108 (1986) 6420.
5 C.A. Tolman, J. Am. Chem. Soc., 92 (1970) 2956.
6 M.M. Rahman, H.Y. Liu, A. Prock and W.P. Giering, Organometallics, 6 (1987) 650.
7 F.G. Mann, A.F. Wells and D. Purdie, J. Chem. Soc., (1937) 1828.
8 C.E. Housecroft, M.L. Buhl, G.J. Long and T.P. Fehlner, J. Am. Chem. Soc., 109 (1987) 3323.
9 L. Casella, M. Gullotti, A. Pintar, F. Pinciroli, R. Viganò and P. Zanello, J. Chem. Soc., Dalton Trans., (1989) 1161.
10 K.S. Wong, W.R. Scheidt and T.P. Fehlner, J. Am. Chem. Soc., 104 (1982) 1111.
11 T.P. Fehlner, C.E. Housecroft, W.R. Scheidt and K.S. Wong, Organometallics, 2 (1983) 825.
12 S.R. Drake, Polyhedron, 9 (1990) 455.
13 P. Zanello, in I. Bernal (Ed.), Stereochemistry of Organometallic and Inorganic Compounds, Elsevier, Amsterdam, 1990, Vol. 5, in press.
14 E.R. Brown and J.R. Sandifer, in B.W. Rossiter and J.F. Hamilton (Eds.), Physical Methods of Chemistry. Electrochemical Methods, J. Wiley, New York, 1986, Vol. 2, ch. 4.